RESEARCH ARTICLE

Flexible Beamforming for Direct Radiating Arrays in Satellite Communications

JUAN ANDRÉS VÁSQUEZ-PERALVO, (Member, IEEE), **JORGE QUEROL**, (Member, IEEE),
FLOR ORTÍZ, (Member, IEEE), **JORGE LUIS GONZÁLEZ RIOS**, (Member, IEEE),
EVA LAGUNAS, (Senior Member, IEEE), **VICTOR MONZON BAEZA**, (Member, IEEE),
GIANLUCA FONTANESI, (Member, IEEE),
LUIS MANUEL GARCÉS-SOCORRÁS, (Member, IEEE),
JUAN CARLOS MERLANO DUNCAN, (Senior Member, IEEE),
AND SYMEON CHATZINOTAS, (Fellow, IEEE)

Interdisciplinary Centre for Security, Reliability and Trust (SnT), L-1855 Luxembourg, Luxembourg

Corresponding author: Juan Andrés Vásquez-Peralvo (juan.vasquez@uni.lu)

ABSTRACT Onboard satellite communication systems generate and manage coverage beams over the Earth. Depending on data traffic requirements, the number of beams, side lobe levels, nulls, and EIRP, their beamwidth must be efficiently generated and managed. Therefore, this paper describes an approach for beam pattern synthesis applied to geostationary satellite communication systems. The beam pattern synthesis can generate beams with a beamwidth variation from $0.45°$ to $1.5°$, which can be controlled independently for the two principal cuts. In addition, other requirements have been considered, e.g., latitude, and longitude, required EIRP, minimum and maximum side love levels for the two principal cuts, and nulling direction. The output of the synthesizer is a weight matrix with beamforming coefficients of the required beam. The direct radiating array in this contribution utilizes an open-ended waveguide antenna as unit cell elements with a period of $0.875\lambda_0$ designed to work in left-hand circular polarization in the frequency band from 17.7 to 20.1 GHz. Since this design is intended for high-data rates applications, the minimum beamwidth requirements are very narrow. Therefore, 36×36 sub-arrays of 4×4 unit cells with a period of 3.5λ are considered to accomplish the beamwidth requirements while maintaining reduced computational and time resources for the weight matrix calculation compared to the conventional counterpart of 144×144 unit cells. The results show that the algorithm, which uses the surrogate optimizer, can compute the weight matrix and synthesize the beam with a slight deviation from the input data.

INDEX TERMS Antennas, beamforming, direct radiating array, satellite communications.

I. INTRODUCTION

Satellite Communications is one of the most essential and robust communication services that allow connecting multiple users, with a line of sight towards the sky, to different internet services. Compared to other communications systems, satellite communications have some critical advantages, e.g., connection in remote areas, emergency services,

Internet of things (IoT) for on-ground sensors, and secure communications, to mention the most relevant.

However, since the increasingly high data rates for different internet applications like video streaming, gaming, and telemedicine, new techniques that allow high data rates are a trending research topic [1]. One of the most straightforward but compelling techniques that enable controlling the data rate for users in a specific area is increasing or decreasing the effective isotropic radiated power (EIRP) for a beam, which implies having higher gain antennas. This has led to advances in antenna on-board technology design, manufacturing, and

The associate editor coordinating the review of this manuscript and approving it for publication was Davide Comite.

control; e.g., magnified phase arrays [2], [3], Direct Radiating Arrays (DRA) [4], and inflatable array antennas [5].

On the other hand, rather than having high-gain antennas with a single beam per feed to cover a determined area with a maximum data rate, nowadays, applications and user requirements have different paradigms where the users are distributed in different locations, with different data rates depending on the day and schedule. Therefore, to amend the previous, beamforming is an essential part of the onboard satellite antenna design, giving control over the beam's position, directivity, power delivered per element, interference control, side lobe levels (SLLs) inside and outside the field of view (FoV), and nulling. Significant advances in beam pattern synthesis over the last 30 years have been made in satellite communication systems. These advances can be classified into two groups. The first group uses deterministic approaches for the beam pattern synthesis, where a mathematical formulation makes the synthesis of the beam, while the second uses optimization or hybrid approaches, combining the deterministic with an optimization tool. Both groups can be subdivided according to the amplitude control over the antenna elements in non-isophoric and isophoric arrays. Isophoric arrays have fixed amplitude in regular and non-regular array elements meaning that the solid-state power amplifiers work at their maximum efficiency while non-isophoric use variable amplitude for each antenna element [6].

Coming back to the first classification group and employing non-isophoric regular arrays, authors have proposed Fourier series [7], amplitude weights [8], [9], [10], [11], [12], polynomial representation [13], and Discrete Fourier Transform (DFT) [14] for beam synthesis. Moreover, combined deterministic approaches for uniform amplitude sparse arrays have been presented in [15].

On the other hand, in the second classification group, plenty of research has been done for non-deterministic array synthesis. For the subdivision of isophoric arrays, authors have synthesized beams using genetic algorithm (GA) for thinned arrays [16] and sparse arrays [17], [18], [19], [20], particle swarm for sparse arrays [21], and mayfly also for sparse arrays [22]. Meanwhile, for the non-isophoric arrays, authors have used genetic algorithms for regular arrays [23], sparse arrays [24], and thinned arrays [25]. In beam synthesis for satellite communication, the first classification has a significant advantage: the reduced time required to produce the required beam. Nevertheless, it is complicated to find a deterministic approach if a beam simultaneously has SLL, beamwidth, nulling, and EIRP constraints. Furthermore, the previous becomes even more complicated when the array uses high-gain sub-arrays associated with it during beam steering. In the state of art, authors have addressed different DRA beam syntheses for satellite communications scenarios. However, they have yet to employ a hybrid approach that considers a DRA with sub-arrays to produce a beam synthesized with the

following input data: SLL and beamwidth in both principal cuts, EIRP, scanning angle, and nulling.

Therefore, this paper presents the following contributions to DRA antenna beam synthesis. First, we consider the effects of using sub-arrays in a beam pattern synthesis and how to compensate for the induced scanning losses, which are much higher than in the not-subarray case. For this purpose, we select a Geostationary Orbit (GEO) study case due to the high antenna gain needed and the convenience of using sub-arrays. Second, we thoroughly present an algorithm that allows synthesizing a radiation pattern considering as input data the beamwidth in two cuts ($\theta_{-3dB_{Az}}$, $\theta_{-3dB_{El}}$), side lobe levels in two cuts (SLL$_{Az}$, SLL$_{El}$), effective isotropic radiated power (EIRP), scanning direction (Λ, Φ), and nulling in a certain direction (θ_{Null}). A comprehensive block diagram of the inputs and outputs of the presented contribution is presented in Figure 1. An interesting approach of this algorithm is combining the tapering approach and deactivating antenna elements to control the desired beamwidth efficiently. Finally, we also present the entire design of a circular polarized open-ended waveguide radiating element from scratch and its integration in the beam pattern synthesis.

This paper is organized as follows. Section II describes the design of the circular polarized radiating element and its co- and cross-polarized radiation pattern, reflection coefficient, and axial ratio simulation results. Section III details the array dimensioning to cover a specific area and the advantages and drawbacks of using sub-array elements as the unit cell of a DRA. Next, a detailed description used for controlling the beamwidth, side lobe levels, and nulling is presented in Section IV. The algorithm and simulation results are described in Section V and Section VI, respectively. The multi-beam scenario is introduced, and an approach is presented in Section VII. Finally, Section VIII presents a set of conclusions and future work derived from this research.

II. ANTENNA DESIGN

In the literature, multiple options exist when selecting an antenna for satellite communications. The antenna type goes in hand with the satellite type, available power, application, frequency, polarization, and expected gain. For instance, and not considering typical solutions like conventional reflector antennas, authors propose using patch antennas [26], [27], [28], [29], reflect array antennas [30], and a combination of both approaches [31]. Other systems consider an improvement in terms of multibeam management by using magnified phase arrays [3]. Nevertheless, nowadays, satellite applications require a high number of beams and directivity with antennas that provide high efficiency; therefore, authors have proposed using horn antennas as radiating elements [32], or open-ended waveguide [33], [34] in a DRA configuration. Hence for this contribution, we select an open-ended waveguide that allows high efficiency and low
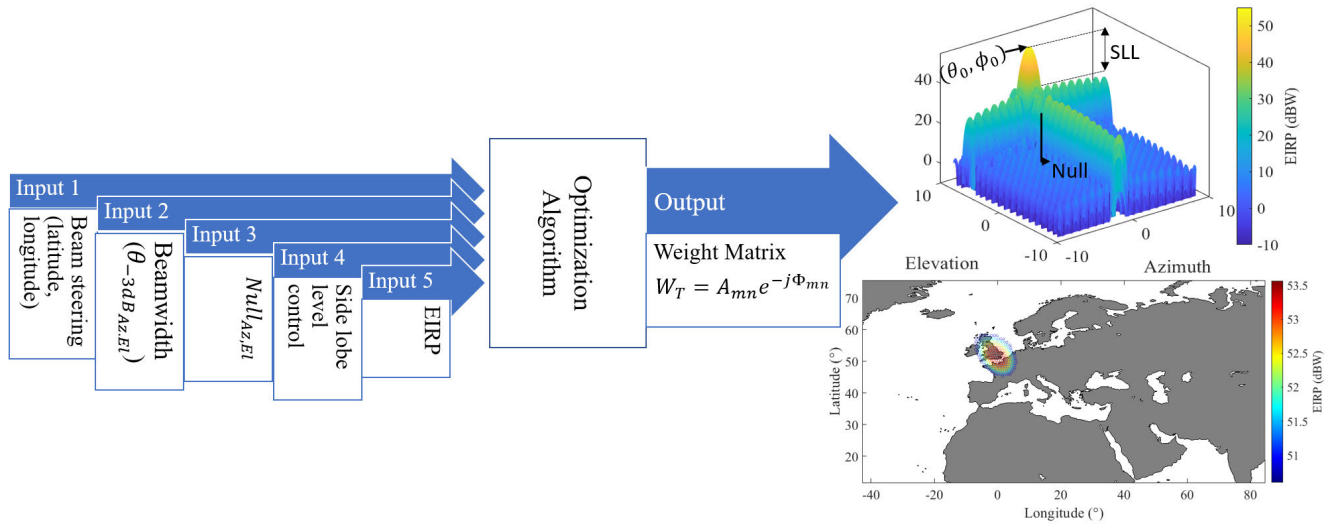
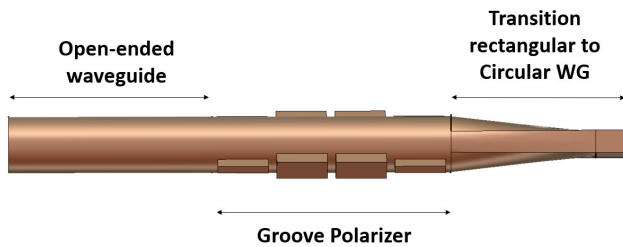**FIGURE 1.** Block diagram of the proposed algorithm.

FIGURE 2. Proposed antenna that includes the open-ended waveguide, groove polarizer, and rectangular to circular waveguide transition.

inter-element separation. The antenna requirements for this contribution were set to an operational band from 17.7 to 20.1 GHz and Left-hand Circular Polarization (LHCP). Following, we will describe the design of the unit cell antenna.

A. TRANSITION AND GROOVE - POLARIZER

Most antennas are fed using a coaxial to rectangular waveguide transition, which gives us an inherently linear polarization (LP). Therefore, a polarization conversion has to be applied to obtain a circular polarization (CP). In our case, and to make our design as realistic as possible, we have designed a rectangular to circular transition and then applied a double-grooved LP-CP mode converter to finally be connected to the antenna, as illustrated in Figure 2.

The rectangular-to-circular waveguide transition will transform the rectangular modes into cylindrical modes by gradually changing the shape of the waveguide from rectangular to circular. The next sections comprise a double grooved mode converter that receives a linear polarized E-Field and generates a 90° phase shifting between two orthogonal modes by placing the grooves at ±45° offset from the diagonal alignment [35].

B. OPEN-ENDED WAVEGUIDE

The final component of this chain comprises the circular open-ended waveguide (COEW), one of the most straight-forward and power-efficient radiating elements. One of the essential features of the COEW is the ability to give us a symmetric beam pattern and allow us to place multiple radiating elements close to each other when working with DRA. Of course, these antennas have some drawbacks, which include the generation of grating lobes in an array configuration, high manufacturing costs, and high profile. Nevertheless, this solution is still worth the drawbacks in terms of power efficiency when working for in-orbit satellite applications. Figure 3 show the dimensions of the optimized antenna, including a rectangular to circular waveguide, double-grooved LP-CP, and an open-ended waveguide.

The antenna was simulated with CST microwave studio using the time domain solver, carefully considering the meshing in the grooves. In addition, we have validated the results by comparing them with another electromagnetic simulator software called high-frequency structure simulator (HFSS). The reflection coefficient, axial ratio, and radiation pattern of the designed antenna are presented in Figure 4. The results show that the antenna maintains an axial ratio below −3 dB and a reflection coefficient below −10 dB in the entire desired bandwidth. Moreover, the radiation pattern obtained has low cross-polarization levels, shown in the RHCP pattern.

Furthermore, the mutual coupling was also analyzed considering two radiating elements placed next to each other at the designed period. The results presented in Figure 5, shows that the coupling between radiating elements is less than −30 dB in the bandwidth of interest.

III. ANTENNA ARRAY DIMENSIONING

The number of DRA elements is tightly related to the required gain, which, in turn, depends on the beam's solid angle, the
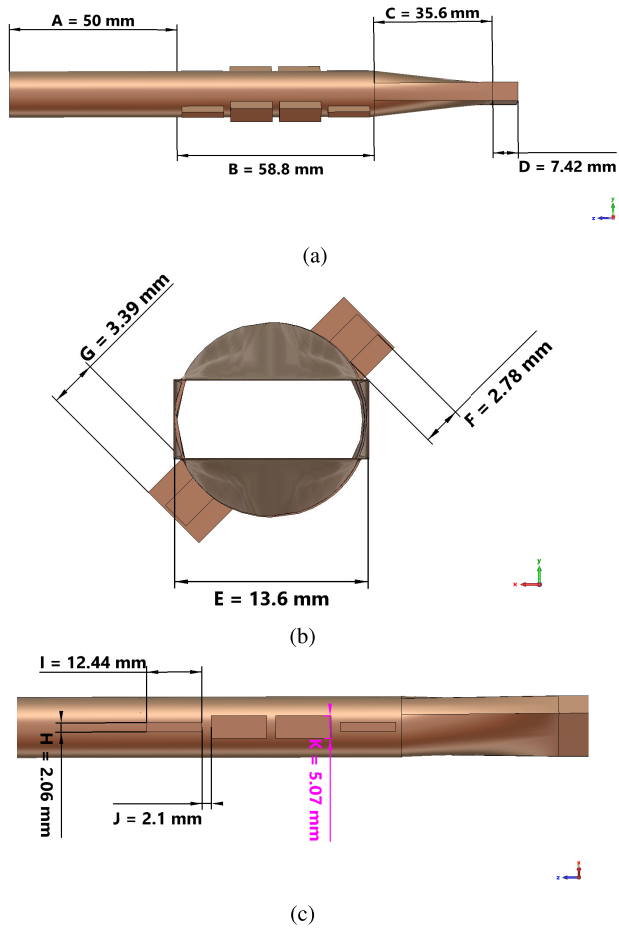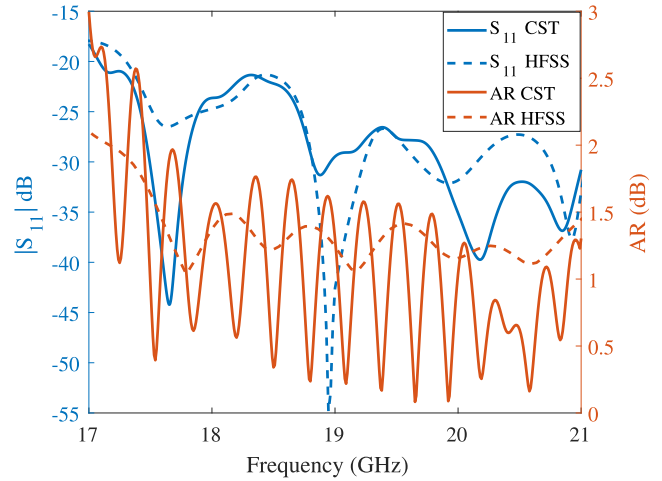
FIGURE 3. Designed antenna dimensions. a) Lateral view. b) Front view. c) Lateral, rotated 45° view.

FIGURE 4. Designed antenna simulation results. a) Reflection coefficient and axial ratio. b) LHCP and RHCP realized gain.
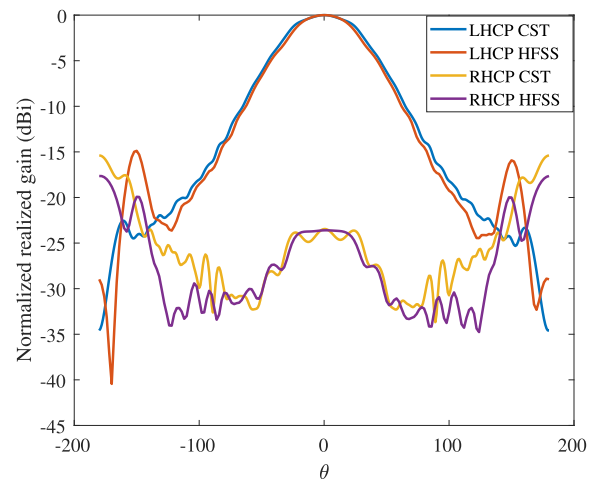
satellite's altitude, position, and coverage area. In this study, we will consider a minimum coverage area of 200000 km^2, and the satellite is located in the geostationary orbit with an orbital position of 13° E. Then, the beamwidth required is 0.45°, which will determine the total number of radiating elements in the DRA. Then, considering that the array is symmetric and rectangular, the number of radiating elements in one dimension to provide the required beamwidth is calculated by (1)

$$N = \frac{\text{asinc}(\frac{1}{\sqrt{2}})\lambda_0}{\eta \, \theta_{-3dB} 2 \, d} \quad (1)$$

where d is the inter-element spacing, λ_0 is the operating wavelength, $\theta_{-3\text{dB}}$ is the beamwidth and η is the antenna efficiency. For this study case, we will consider an inter-element separation of $7/8\lambda_0$ to have a mutual coupling below -30 dB for a central frequency $f_0 = 19$ GHz. To estimate the efficiency of this array, one approach would be to use full-wave simulations, but this can be computationally intensive and resource-consuming. Alternatively, we can estimate the array efficiency by considering the efficiency of each unit cell. In this case, the simulated efficiency of the unit cell was found

to be approximately 97% in the frequency band of interest. However, to account for other potential factors that could impact the overall efficiency of the array, it is recommended to use a conservative estimate of 90% for future calculations. Finally, and using the previous values, the number of elements for the proposed DRA is 144 × 144.

The large number of required elements in our design would make practical implementation prohibitively expensive, significantly increase power requirements, and necessitate a larger physical footprint. One way to reduce the total number of elements and keep a high gain and beamwidth characteristics is using sub-arrays. In our case, we can highly reduce the total number of RF chains, to 36 × 36, by using 4 × 4 elements sub-arrays. Therefore, considering the new unit cell dimension, the new inter-element space in the array is 3.5λ_0. If we simulate both scenarios, with and without sub-arrays, we can find some interesting results that should be considered in beamforming optimization. First, the normalized radiation
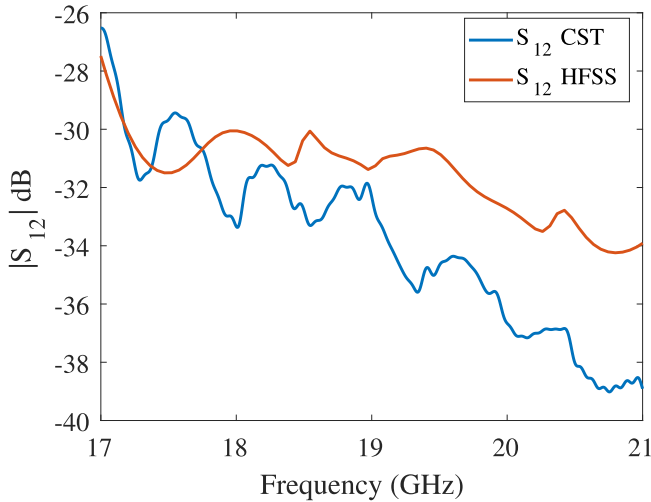
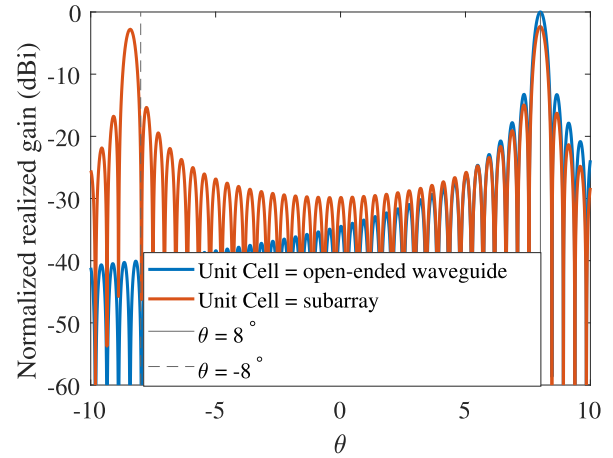**FIGURE 5.** Calculated Mutual coupling considering two radiating elements presented in Figure 3, separated 7/8λ.
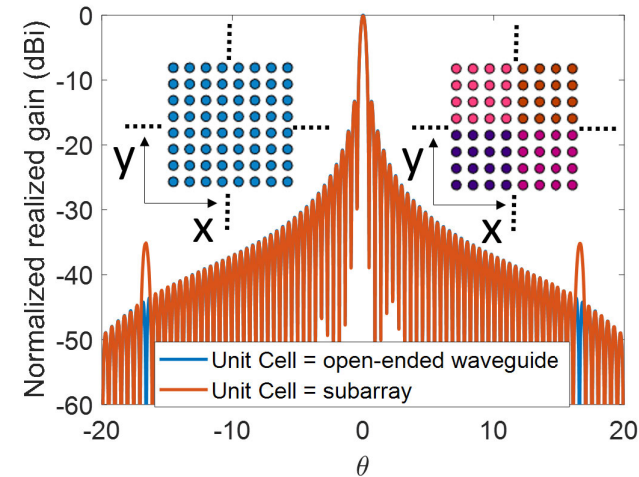

FIGURE 6. Normalized radiation pattern of an array of 144 × 144 unit cells and an array of 36 × 36 sub-arrays. Only 8 × 8 out of 144 × 144 elements are represented for the array scenario (left), and 2 × 2 out of 36 × 36 elements are represented for the sub-array scenario (right).

pattern with a scanning angle (0°, 0°) is illustrated in Figure 6. In this simulation, we can see that the main beam, in both scenarios, is quite similar, with a slight reduction in the sub-array case due to the grating lobes generated by the new period of the array unit cell.

Second, lets us consider the scenario where the scanning angle is (0°, 8°) illustrated in Figure 7. We can see two differences in the radiation pattern results: reduced gain and marked grating lobes in the sub-array case. Considering the first effect, we must address this reduction when working with the EIRP values since it depends on the antenna gain. The second, for our application, grating lobes will not affect the illumination over the earth since it is outside the field of view, validating the correct dimensioning of the DRA.

FIGURE 7. Normalized radiation pattern of an array of 144 × 144 unit cells and an array of 36 × 36 sub-arrays scanning to an angle (0°, 8°). The normalization uses the reference of the open-ended waveguide case.

IV. BEAMWIDTH, SLL, NULLING, AND EIRP CONTROL

Next, a short description of the main parameters we want to control in the optimization process is presented. It is worth mentioning that the progressive phase shift and nulling are not directly optimized parameters since their calculation is straightforward. Still, they must be considered essential elements since the scanning losses, and a null will modify the EIRP and SLL, respectively.

A. SCANNING ANGLES

Steering a beam is a straightforward process that involves modifying the complex component of the weight matrix. One of the most used approaches to beam steering is generating a progressive phase shift in each DRA element. Other options use an N-point FFT [36], [37] or codebook-based beamforming [38]; both are used for fixed multi-beam scenarios. For instance, if we need to place the main beam in the position corresponding to latitude 40.41°, longitude 3.70° and the satellite is located at 13°E, applying the coordinate transformation from latitude and longitude to azimuth and elevation, the antenna needs to point to an azimuth −1.8° and elevation 5.3°, as illustrated in Figure 8a. Then if we use the incremental phase shift formula (2)

$$\Theta_{mn} = k(md_x \sin(\theta_0)\cos(\phi_0) + nd_y \sin(\theta_0)\sin(\phi_0)), \quad (2)$$

where k is the wave number, m and n are the positions of the elements in the x and y-axis, respectively, d_x and d_y are the corresponding periods, and θ_0 and ϕ_0 are the scanning angles; we can calculate incremental phase shift to steer the main beam, which is 0.6908° and 2.0313° in the x- and y-axis, respectively. The designed beam can be easily projected over the earth by doing the same coordinate transformation starting from the azimuth - elevation coordinates, Figure 8a, changing it to U-V coordinates, Figure 8b, and, finally, to latitude and longitude, Figure 8c.
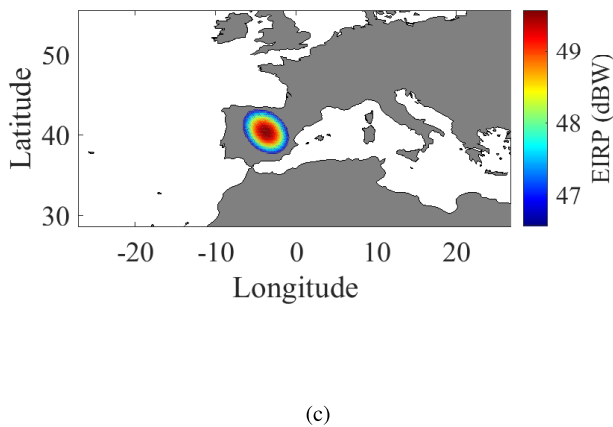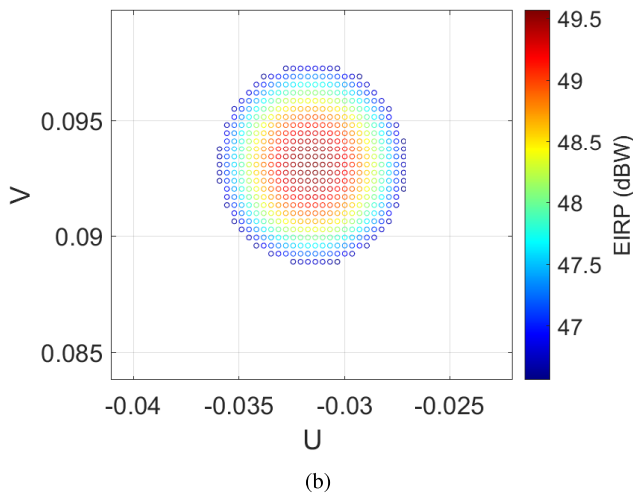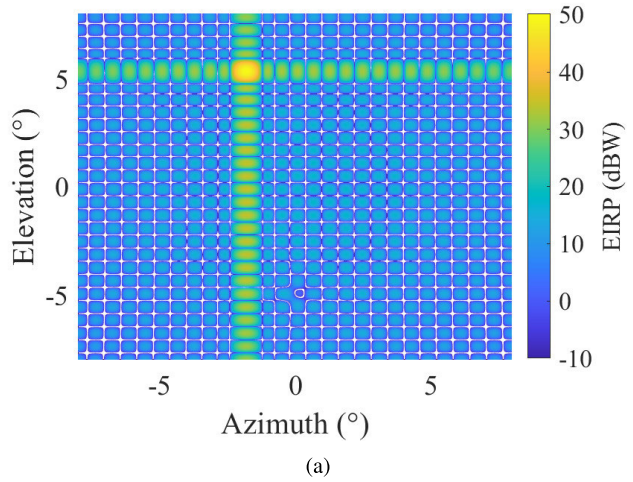
(a)

(b)

(c)

FIGURE 8. Main beam radiation pattern at −3 dB of a DRA of 36 × 36 elements presented in Figure 7, at different coordinate systems. a) Azimuth - Elevation. b) U-V. c) Latitude - Longitude.

B. BEAMWIDTH AND SLL CONTROL

Different techniques control the beamwidth and SLL of the main beam. Tapering controls the SLL by modifying the amplitude weight of each element, and usually, it is a
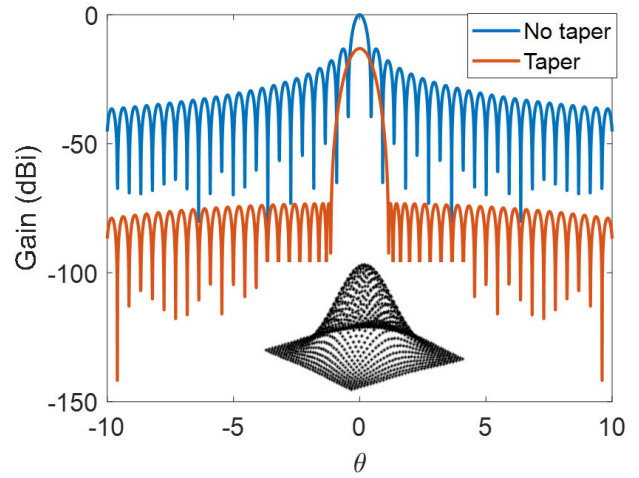

FIGURE 9. Tapered and un-tapered radiation pattern of a 32 × 32 sub-array elements radiating at broadside.

function of the position of the unit cell and decreases with length. In our case, we will control both using a Chebyshev amplitude tapering due to its high narrowing of the beam characteristics compared to other tapering options. Chebyshev amplitude tapering uses Chebyshev's polynomials to calculate the amplitude weight of the DRA; detailed information on Chebyshev's amplitude tapering can be found in [39]. An example of a Chebyshev taper with a reduction of SLL to 60 dB and their effects over the previously analyzed DRA radiation pattern is illustrated in Figure 9.

Analyzing Figure 9, we can see that as we increase the desired SLL, the antenna's gain decreases, and the beamwidth increases. Therefore, tapering allows for controlling beamwidth and SLL levels in azimuth and elevation of the radiation pattern. Finally, addressing an exact beamwidth involves an optimization process, especially if we deactivate entire rows and columns at the edges to easily and efficiently address the desired beamwidth and the EIRP when compensating for losses in a beam scanning scenario. This process will be explained in the next section.

C. NULLING CONTROL

Placing one or multiple nulls can be controlled easily by modifying the antenna progressive phase shift by generating a null beam in the desired direction and subtracting it from the original radiation pattern. This concept in a mathematical expression can be written as

$$W_T = W_{\theta_0\phi_0} - W_{\text{null}} \left(\frac{W'_{\text{null}} W_{\theta_0\phi_0}}{W'_{\text{null}} W_{\text{null}}} \right), \qquad (3)$$

where $W_{\theta_0\phi_0}$ is the weight matrix with the progressive phase shift to the steering direction and W_{null} is the weight matrix with the progressive phase shift towards the desired nulling angle. To picture this concept, let us consider the previous case where the antenna needs to point at the broadside and place a null at (0°, 5°). The result of applying (3) to obtain the final weight matrix is illustrated in Figure 10.
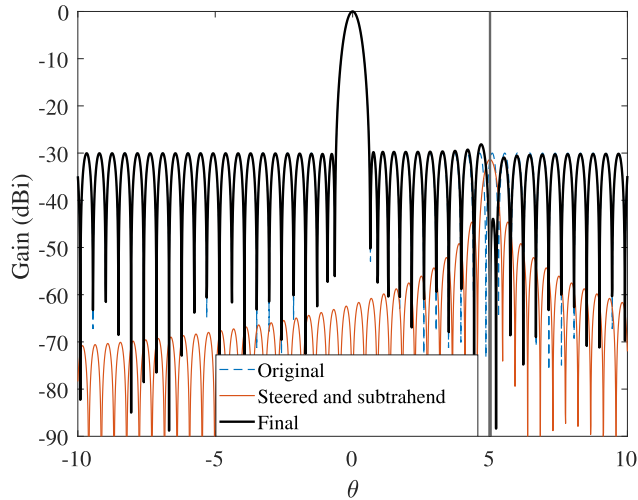
FIGURE 10. Normalized radiation pattern of an array of 36×36 sub-arrays with a null at $(0°, 5°)$. The graphic also includes the step-by-step generation of the null.

D. EIRP CONTROL

The EIRP control of the DRA is a function of the beamwidth, scanning angle, and the power radiated by each antenna element. Considering the beamwidth, as explained before, it can be optimized by the SLL control if a tapering function is applied or by variating the number of active rows and columns. Furthermore, in a beam scanning scenario that uses subarrays as radiating elements, the main beam will follow the contour of the unit cell element pattern, in our case, the radiation pattern of a 4×4 elements sub-array. This will induce an important reduction in the main beam directivity when the scanning angle differs from the broadside. For instance, let us consider the example presented in Figure 7. The array is scanning at $(0°, 8°)$, giving scanning losses around 2.4 dB compared to the non-subarray case. If we desired an EIRP equal to the case $(0°, 0°)$, the losses associated with these scanning angles must be compensated by dynamically increasing the power per element.

On the other hand, there is another scenario where the required beamwidth is very narrow, leading to a higher gain resulting in a bigger EIRP than the desired. In this case, the algorithm will reduce the power per element to address the required EIRP. It is worth mentioning that the proposed algorithm not just compensates for the scanning losses by increasing the power per element, but it also compensates it based on the active antenna elements, which are associated with the desired beamwidth and SLLs. The previous also applies to the case where narrow beamwidths generate bigger EIRP than the desired ones.

V. BEAMFORMING ALGORITHM

In the previous sections, we have addressed the basic concepts and techniques to control beam scanning, beamwidth, SLL, EIRP, and nulling of a DRA radiation pattern. Working with all this together requires the help of an optimization tool. For instance, let us consider the scenario presented in Section II. The antenna must provide a symmetric beam pointing to latitude 51.6627°, longitude −0.13363°, with $\theta_{-3dB} = 1°$. To avoid interference with other beams, the SLL has to be in the range $16 \geq SLL \leq 25$. Nulling must be placed in the adjacent beam located in latitude 28.3105°, longitude 4.1379°. Finally, the EIRP required for this beam is 53 dBW. Analyzing the requirements, we can control the beamwidth by tapering and deactivating rows and columns. In addition, there are constraints in SLL that also can be addressed by proper tapering with a fair number of active elements. Moreover, when applying nulling, the SLL of the nearest secondary lobe is increased, as described in the previous section. Finally, even though generating the correct scanning angle is a straightforward process, we have to consider that in the case of sub-arrays, the antenna gain is reduced as the scanning angle increases. Therefore, that reduction has to be compensated to address the required EIRP. Concretely, to address the previous requirements, a beamforming algorithm has been implemented, and the most suitable optimizer for this work is the surrogate optimizer. The optimizer will minimize the cost function $F(Z_1 + Z_2 + Z_3)$, where each element is described in (4), by variating the number of active rows and columns in the array, selecting the adequate SLL in both planes using tapering to generate the required θ_{-3dB}, and computing the required power per element to address the necessary EIRP. The cost function is composed of a sum of three sub-objectives. The first will describe the error between both cuts desired $\theta_{-3dB_{El_o}}^B$, $\theta_{-3dB_{Az_o}}^B$ and calculated $\theta_{-3dB_{El_c}}^B$, $\theta_{-3dB_{Az_c}}^B$ beamwidth per beam. The second will calculate in both cuts the error between the minimum $SLL_{Az_o}^b$, $SLL_{El_o}^b$ and the calculated $SLL_{Az_c}^b$, $SLL_{El_c}^b$. Finally, the last term calculates the error between the desired $EIRP_o^b$ and the calculated $EIRP_c^b$. Each of those terms has a weighting factor k_1, k_2, k_3 that will add additional weight to their calculation.

The beamforming algorithm used is described in Algorithm (1), and the algorithm thinking process is given below.

- **Coordinate transformation:** The latitude and longitude positions are transformed into azimuth and elevation coordinates visible to the antenna.
- **Initial weight matrix:** The progressive phase shift, nulling, and tapering based on Chebyshev amplitude control are calculated to generate an initial weight matrix W_o^B that includes all active elements, and an initial power per element PPE.
- **Radiation pattern extraction:** The algorithm calculates the radiation pattern principal cuts for each beam in each iteration and extracts the beamwidth, side lobe level, nulling, and EIRP for both cuts.
- **Cost function calculation:** Based on the extracted parameters, the algorithm calculates the cost function F. If the cost function is lower than the minimum threshold, the algorithm stops, and the optimum weight matrix $W_{p \times q}^B$ is output as the result.

Algorithm 1 Beam Forming Algorithm

Input: (Λ^B, Φ^B), center of the beam in Latitude and
   longitude coordinates per beam,
   $\theta_{-3dB_{Az}^B}$, beamwidth cut in azimuth per beam,
   $\theta_{-3dB_{El}^B}$, beamwidth cut in elevation per beam,
   $EIRP^B$, EIRP per beam,
   SLL_{min}^B, SLL minimum per beam,
   SLL_{max}^B, SLL maximum per beam,
   $(\theta_{Null}^B, \phi_{Null}^B)$, Null position per beam
Output: $W_{p \times q}^B$, Weight matrix based on previous
   inputs
Data: Set of possible configurations on Satellite
   considering system constraints

1 **Initiate:** Surrogate Optimizer
2 **if** counter < counter$_{max}$ **then**
3 | **Calculate:** W_o^B
4 | **Calculate:** radiation pattern, $\theta_{-3dB_{El}^B}$, $\theta_{-3dB_{Az}^B}$,
   | SLL_{min}^B, *and* $EIRP^B$
5 | **Calculate:** $F(Z_1 + Z_2 + Z_3)$
6 | **if** $F < F_{min}$ **then**
7 | | $W_{p \times q}^B = W_o^B$
8 | | saves the optimal matrix
9 | | **break**
10 | **else**
11 | | counter $\leftarrow$ counter + 1;
12 | **Optimize:** p, q, SLL_{Az}, SLL_{El}, *and* PPE

- **Optimization:** If the cost function is above the threshold, the algorithm increases the counter and searches for a suitable active number of rows p, columns q, a Chebyshev taper based on the allowable side lobe level range, and power per element PPE. The previous steps and calculations are repeated until the optimal weight matrix is found.

$$\min_{W_{p \times q}^B} Z_1(W_{p \times q}^B) + Z_2(W_{p \times q}^B) + Z_3(W_{p \times q}^B), \quad (4)$$

where

$$
\begin{cases}
Z_1 = \left(\dfrac{|\theta_{-3dB_{Az_c}}^b(W_{p \times q}^B) - \theta_{-3dB_{Az_o}}^b|}{\theta_{-3dB_{Az_o}}^b} \right. \\
\qquad \left. + \dfrac{|\theta_{-3dB_{El_c}}^b(W_{p \times q}^B) - \theta_{-3dB_{El_o}}^b|}{\theta_{-3dB_{El_o}}^b} \right) k_1 \\[2mm]
Z_2 = \left(\dfrac{|SLL_{Az_c}^b(W_{p \times q}^B) - SLL_{Az_o}^b|}{SLLAz_o^b} \right. \\
\qquad \left. + \dfrac{|SLL_{El_c}^b(W_{p \times q}^B) - SLL_{El_o}^b|}{SLLEl_o^b} \right) k_2 \\[2mm]
Z_3 = \left(\dfrac{EIRP_c^b(W_{p \times q}^B) - EIRP_o^b}{EIRP_o^b} \right) k_3,
\end{cases}
$$

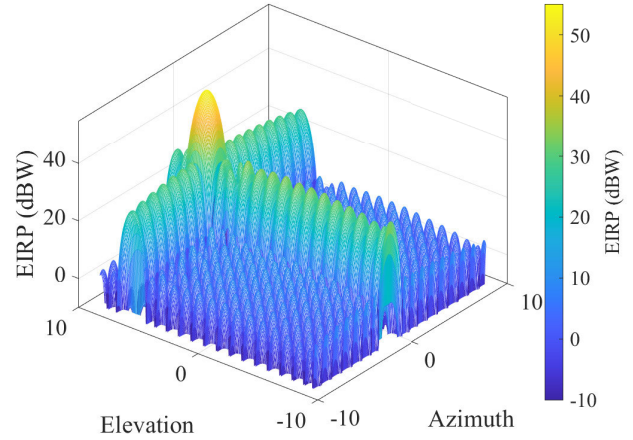Finally, the computational complexity of the proposed algorithm is primarily influenced by the number of antenna

FIGURE 11. 3D Radiation pattern results of a beam with a $\theta_{-3dB_{Az}} = \theta_{-3dB_{El}} = 1°$, pointing to latitude 51.66274°, longitude $-0.13363°$, with a null at latitude 28.3910°, longitude $-4.1302°$, providing an EIRP = 53 dBW.

elements received as input. This algorithm employs the AF (Array Factor) formula to estimate the approximate radiation pattern for subsequent calculations of beamwidth, SLL (Side Lobe Level), nulls, and EIRP (Effective Isotropic Radiated Power). As the total number of antenna elements increases, the algorithm's runtime also grows due to the need for larger matrices and more multiplications involved in the array factor computation. However, the computational complexity is significantly reduced when considering the sub-array scenario. In this case, the algorithm benefits from a smaller set of antenna elements, reducing the size of matrices and the number of required multiplications. Specifically, the computational complexity decreases by N^2, where N represents the sub-array size.

VI. RESULTS

A. BEAMFORMING ALGORITHM

The results have been obtained using the unit cell radiation pattern previously obtained in CST Microwave Studio and exported to Matlab, where the optimization algorithm, beamwidth, SLL, EIRP, sub-array, and array patterns have been implemented to obtain the final radiation pattern.

The radiation pattern calculated using the algorithm previously presented is illustrated in Figure 11, and the principal cuts result in Figure 12.

As can be seen, after the coordinate transformation, the radiation pattern main beam is scanning at Az = $-1.1459°$, El = 6.3504° and a null is located at Az = $-1.1459°$, El = 4.05°. The weight matrix amplitude distribution shows that the algorithm deactivates 20 rows and columns to address the required beamwidth and SLL, as illustrated in Figure 13. Finally, in order to project the optimized radiation pattern, shown in Figure 11 onto the earth's surface, a coordinate transformation was performed from azimuth-elevation to latitude-longitude. The resulting projection, which only
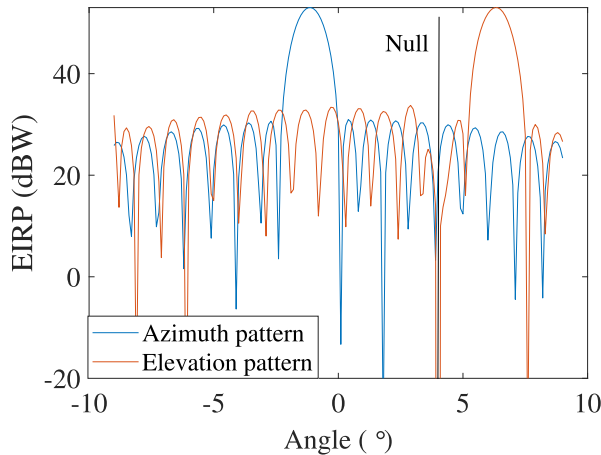
FIGURE 12. Principal cut results of a beam with a $\theta_{-3dB_{Az}} = \theta_{-3dB_{El}} = 1°$, pointing to latitude 51.66274°, longitude −0.13363°, with a null at latitude 28.3910°, longitude −4.1302°, providing an EIRP = 53 dBW.
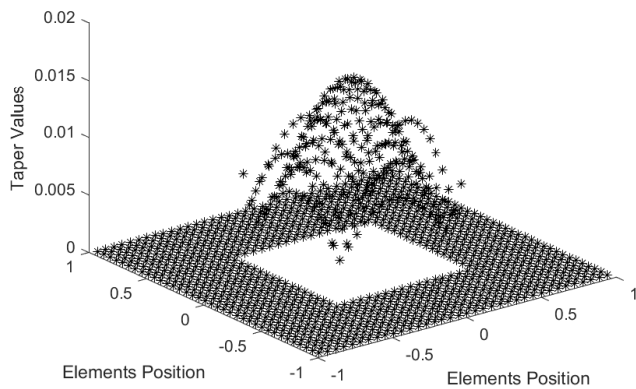

FIGURE 13. DRA amplitude taper corresponding to the radiation pattern presented in Figure 12.

FIGURE 14. Projection over the earth in latitude and longitude coordinates, corresponding to the radiation pattern presented in Figure 11. The resulting projection only considers up to the half-power points of the radiation pattern.
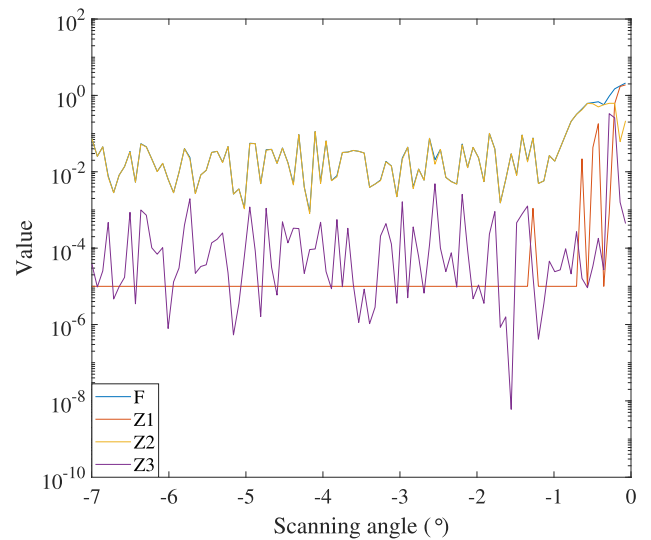
FIGURE 15. Algorithm performance as the scanning angle approaches a null in the scanning region. y-axis is in logarithmic scale.

takes into account up to the half-power points, is shown in Figure 14. This figure clearly demonstrates that the beam is centered at the intended latitude and longitude, but has a wider and tilted shape. The deformation is primarily due to the position of the satellite and the curvature of the earth.

The effectiveness of the algorithm has been tested in multiple scenarios. The three most relevant scenarios are analyzed in this paper, and the inputs and results are presented in Table 1. For easy calculation, the latitude and longitude values have been replaced directly with a calculated azimuth and elevation angle.

1) The first scenario considers the case where the required beam has to have high directivity, which means a very narrow beamwidth. In addition, the scanning angle is set to (8°,8°), and the EIRP to 59 dBW. As a result, the synthesized radiation pattern shows a very low deviation from the input data, having a maximum error of around 0.48%. In addition, and this applies to other cases, there is no error in the scanning direction between the input and output data. This is due to
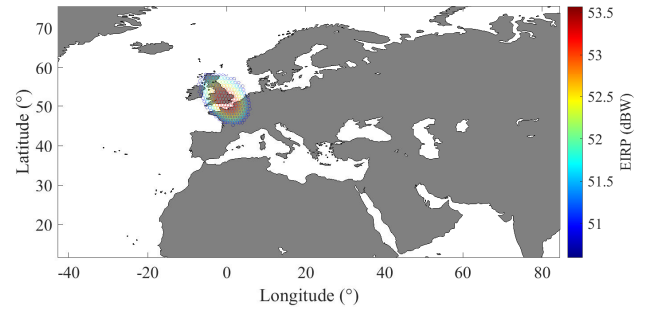
the straightforward use of the progressive phase shift formula.

2) The second case has the same input as the previous but scanning at broadside. In this case, and as analyzed previously, the losses are lower, which implies that the power per element needed will decrease.

3) The last case considers the opposite of case one, being a beam with the maximum available beamwidth. Since the algorithm finds power efficiency, it will turn off rows and columns rather than apply tapering to the whole structure to address the beamwidth requirements. Moreover, since the EIRP requirements are the same as the previous cases, the power per element required is greater, reaching 41.75 dBm.

B. ALGORITHM PERFORMANCE

To evaluate the algorithm's effectiveness, we can use $F(Z_1 + Z_2 + Z_3)$ as a figure of merit because the algorithm's objective

TABLE 1. Simulation results using the surrogate optimizer in three different scenarios.

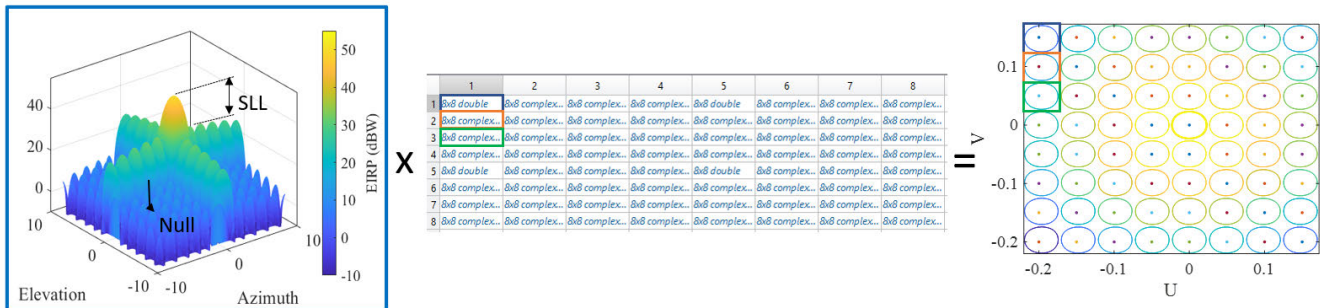|		$\theta_{-3dB_{Az}}$ (°)	$\theta_{-3dB_{El}}$ (°)	SLL_{Az} (dB)	SLL_{El} (dB)	Az (°)	El (°)	EIRP (dBW)	Power per element (dBm)	Active rows
Case 1	Input	0.45	0.45	———	———	8	8	49	———	———
	Output	0.44778	0.45178	17.575	18.835	8	8	49.003	6.6	34
Case 2	Input	0.45	0.45	———	———	0	0	49	———	———
	Output	0.45038	0.44637	22.398	21.821	0	0	49.008	2.53	34
Case 3	Input	1.5	1.5	———	———	-8	-8	49	———	———
	Output	1.495	1.4965	24.006	24.885	-8	-8	49.018	41.75	12

FIGURE 16. Multi-beam scenario using an 8-point FFT.

is to minimize it, making it a good performance metric. For instance, let's consider testing the effectiveness of the algorithm as we scan the main beam from (−7°, 0°) to (0°, 0°), placing a null at (0°, 0°), and having a beamwidth of 1°. In this case, the algorithm's performance is degraded as the main beam approaches the nulling region. To illustrate this, Figure 15 shows the value of each function component *F* and how it changes at each iteration. As shown in the figure, in the range from (−7°, 0°) to (0°, 0°), the algorithm does a good job of placing F under 0.08. However, as we go further to −1°, the beamwidth error metric worsens due to the null position. Additionally, as we approach 0°, the SLL error metric suddenly increases due to the fake side lobe generated by the split of the main beam. Finally, it can be seen that the power, in this case, does not address the requirements in the region where the beam splits.

VII. MULTI-BEAM SCENARIO

The application of the proposed algorithm can be extended to a multibeam scenario. For instance, let us consider a 64-beam scenario of 8 × 8 equally spaced beams with equal characteristics in terms of beamwidth, EIRP, SLL, and nulling. The proposed algorithm can obtain the required weight matrix that addresses the beamwidth, EIRP, SLL, and nulling, and, to control the steering, we can use an 8-point FFT to calculate the additional weight matrix. Finally, the final weight matrix for each beam can be calculated by multiplying previously calculated weight matrices. This process is illustrated in Figure 16. Furthermore, this concept can be extended to cases where the beams do not necessarily have the same characteristics. In that case, the algorithm should calculate the weight matrix for each required beam.

VIII. CONCLUSION

A beam synthesize optimization algorithm that computes an optimized weight matrix receiving as an input: beamwidth, side lobe levels, nulling, and effective isotropic radiated power for a DRA for satellite communications has been proposed, dimensioned, designed, and simulated. The DRA design takes a Geostationary Orbit satellite as a case study, delivering a narrow beamwidth with low cross-polarization. In addition, the DRA is designed using open-ended waveguides that uses a groove polarizer to achieve the required circular polarization. The proposed DRA uses sub-arrays to enhance the directivity while reducing the number of RF chains, which relaxes computational resources and simulation time. Moreover, using sub-arrays will also highly reduce cost, mass, and power in a practical implementation. Furthermore, this algorithm does not limit to one beam, it can be used for a multi-beam scenario with different requirements considering an N-point FFT or beamforming codebook.

The amplitude of the weight matrix needed to address the previous parameters is calculated using the surrogate optimizer, which will determine the best suitable number of active rows and columns, amplitude tapering, and power per element; meanwhile, the weight matrix phase is computed based on the beam scanning and nulling, which are calculated using progressive phase shift and beam suppression, respectively. Finally, the obtained results can be computed for different scenarios variating the beamwidth, SLL range, EIRP, nulling to be used in the future as training data for machine learning applications.

ACKNOWLEDGMENT

REFERENCES

[1] O. Kodheli, E. Lagunas, N. Maturo, S. K. Sharma, B. Shankar, J. F. M. Montoya, J. C. M. Duncan, D. Spano, S. Chatzinotas, S. Kisseleff, J. Querol, L. Lei, T. X. Vu, and G. Goussetis, "Satellite communications in the new space era: A survey and future challenges," *IEEE Commun. Surveys Tuts.*, vol. 23, no. 1, pp. 70–109, 1st Quart., 2021.

[2] F. Pelorossi, G. Toso, and P. Angeletti, "On the scanning properties of imaging antennas based on dual confocal paraboloidal reflectors," *Prog. Electromagn. Res. M*, vol. 37, pp. 95–107, 2014.

[3] C. Sciannella and G. Toso, "An imaging reflector system with reduced scanning aberrations," *IEEE Trans. Antennas Propag.*, vol. 63, no. 4, pp. 1342–1350, Apr. 2015.

[4] A. F. Morabito, T. Isernia, M. G. Labate, M. Durso, and O. M. Bucci, "Direct radiating arrays for satellite communications via aperiodic tilings," *Prog. Electromagn. Res.*, vol. 93, pp. 107–124, 2009.

[5] J. Huang, "The development of inflatable array antennas," *IEEE Antennas Propag. Mag.*, vol. 43, no. 4, pp. 44–50, Aug. 2001.

[6] D. G. Leeper, "Isophoric arrays-massively thinned phased arrays with well-controlled sidelobes," *IEEE Trans. Antennas Propag.*, vol. 47, no. 12, pp. 1825–1835, Dec. 1999.

[7] S. A. Schelkunoff, "A mathematical theory of linear arrays," *Bell Syst. Tech. J.*, vol. 22, no. 1, pp. 80–107, Jan. 1943.

[8] C. L. Dolph, "A current distribution for broadside arrays which optimizes the relationship between beam width and side-lobe level," *Proc. IRE*, vol. 34, no. 6, pp. 335–348, Jun. 1946.

[9] T. T. Taylor, "Design of line-source antennas for narrow beamwidth and low side lobes," *Trans. IRE Prof. Group Antennas Propag.*, vol. 3, no. 1, pp. 16–28, Jan. 1955.

[10] R. B. Blackman and J. W. Tukey, "The measurement of power spectra from the point of view of communications engineering—Part I," *Bell Syst. Tech. J.*, vol. 37, no. 1, pp. 185–282, Jan. 1958.

[11] R. Webster, "A generalized Hamming window," *IEEE Trans. Acoust., Speech, Signal Process.*, vol. ASSP-26, no. 3, pp. 269–270, Jun. 1978.

[12] L. D. Fielder, M. Bosi, G. Davidson, M. Davis, C. Todd, and S. Vernon, "AC-2 and AC-3: Low-complexity transform-based audio coding," *J. Audio Eng. Soc.*, May 1996.

[13] H. J. Orchard, R. S. Elliott, and G. J. Stern, "Optimising the synthesis of shaped beam antenna patterns," *IEE Proc. H, Microw., Antennas Propag.*, vol. 132, no. 1, pp. 63–68, 1985.

[14] H.-T. Chou, Y.-T. Hsaio, P. H. Pathak, P. Nepa, and P. Janpugdee, "A fast DFT planar array synthesis tool for generating contoured beams," *IEEE Antennas Wireless Propag. Lett.*, vol. 3, pp. 287–290, 2004.

[15] O. M. Bucci, M. D'Urso, T. Isernia, P. Angeletti, and G. Toso, "Deterministic synthesis of uniform amplitude sparse arrays via new density taper techniques," *IEEE Trans. Antennas Propag.*, vol. 58, no. 6, pp. 1949–1958, Jun. 2010.

[16] R. L. Haupt, "Thinned arrays using genetic algorithms," *IEEE Trans. Antennas Propag.*, vol. 42, no. 7, pp. 993–999, Jul. 1994.

[17] O. M. Bucci and D. Pinchera, "A generalized hybrid approach for the synthesis of uniform amplitude pencil beam ring-arrays," *IEEE Trans. Antennas Propag.*, vol. 60, no. 1, pp. 174–183, Jan. 2012.

[18] G. Toso, C. Mangenot, and A. G. Roederer, "Sparse and thinned arrays for multiple beam satellite applications," in *Proc. 2nd Eur. Conf. Antennas Propag. (EuCAP)*, 2007, pp. 1–4.

[19] O. M. Bucci, T. Isernia, S. Perna, and D. Pinchera, "Isophoric sparse arrays ensuring global coverage in satellite communications," *IEEE Trans. Antennas Propag.*, vol. 62, no. 4, pp. 1607–1618, Apr. 2014.

[20] O. M. Bucci, S. Perna, and D. Pinchera, "Synthesis of isophoric sparse arrays allowing zoomable beams and arbitrary coverage in satellite communications," *IEEE Trans. Antennas Propag.*, vol. 63, no. 4, pp. 1445–1457, Apr. 2015.

[21] Y.-F. Cheng, X. Ding, W. Shao, and C. Liao, "A high-gain sparse phased array with wide-angle scanning performance and low sidelobe levels," *IEEE Access*, vol. 7, pp. 31151–31158, 2019.

[22] E. O. Owoola, K. Xia, T. Wang, A. Umar, and R. G. Akindele, "Pattern synthesis of uniform and sparse linear antenna array using mayfly algorithm," *IEEE Access*, vol. 9, pp. 77954–77975, 2021.

[23] K.-K. Yan and Y. Lu, "Sidelobe reduction in array-pattern synthesis using genetic algorithm," *IEEE Trans. Antennas Propag.*, vol. 45, no. 7, pp. 1117–1122, Jul. 1997.

[24] M. Viganö, G. Toso, P. Angeletti, I. Lager, A. Yarovoy, and D. Caratelli, "Sparse antenna array for Earth-coverage satellite applications," in *Proc. 4th Eur. Conf. Antennas Propag.*, 2010, pp. 1–4.

[25] G. Caille, Y. Cailloce, C. Guiraud, D. Auroux, T. Touya, and M. Masmousdi, "Large multibeam array antennas with reduced number of active chains," in *Proc. 2nd Eur. Conf. Antennas Propag. (EuCAP)*, 2007, p. 142.

[26] K. Y. Kapusuz, Y. Şen, M. Bulut, I. Karadede, and U. Oğuz, "Low-profile scalable phased array antenna at Ku-band for mobile satellite communications," in *Proc. IEEE Int. Symp. Phased Array Syst. Technol. (PAST)*, Oct. 2016, pp. 1–4.

[27] A. H. Aljuhani, T. Kanar, S. Zihir, and G. M. Rebeiz, "A 256-element Ku-band polarization agile SATCOM receive phased array with wide-angle scanning and high polarization purity," *IEEE Trans. Microw. Theory Techn.*, vol. 69, no. 5, pp. 2609–2628, May 2021.

[28] S. Abulgasem, F. Tubbal, R. Raad, P. I. Theoharis, S. Lu, and S. Iranmanesh, "Antenna designs for CubeSats: A review," *IEEE Access*, vol. 9, pp. 45289–45324, 2021.

[29] F. E. Tubbal, R. Raad, and K.-W. Chin, "A survey and study of planar antennas for pico-satellites," *IEEE Access*, vol. 3, pp. 2590–2612, 2015.

[30] Y. Li, Z. H. Jiang, X. Tong, F. Wu, N. Shen, R. Sauleau, and W. Hong, "Wideband dual-circularly-polarized reflect-arrays based on dual-functional-layer cells with berry-phase compensation at X-band," *IEEE Trans. Antennas Propag.*, vol. 70, no. 10, pp. 9924–9929, Oct. 2022.

[31] Y. Yao, X. Q. Lin, T. Qin, Y. Su, and X. Yang, "Shared-aperture Ka-band reflectarray and X-band phased array for broadband inter-satellite communication," *IEEE Trans. Antennas Propag.*, vol. 70, no. 11, pp. 11199–11204, Nov. 2022.

[32] S.-M. Moon, S. Yun, I.-B. Yom, and H. L. Lee, "Phased array shaped-beam satellite antenna with boosted-beam control," *IEEE Trans. Antennas Propag.*, vol. 67, no. 12, pp. 7633–7636, Dec. 2019.

[33] C. Kumar, V. V. Srinivasan, V. K. Lakshmeesha, and S. Pal, "Novel dual circularly polarized radiating element for spherical phased-array application," *IEEE Antennas Wireless Propag. Lett.*, vol. 8, pp. 826–829, 2009.

[34] C. Kumar, B. P. Kumar, V. S. Kumar, and V. V. Srinivasan, "Dual circularly polarized spherical phased-array antenna for spacecraft application," *IEEE Trans. Antennas Propag.*, vol. 61, no. 2, pp. 598–605, Feb. 2013.

[35] N. Yoneda, R. Miyazaki, I. Matsumura, and M. Yamato, "A design of novel grooved circular waveguide polarizers," *IEEE Trans. Microw. Theory Techn.*, vol. 48, no. 12, pp. 2446–2452, Dec. 2000.

[36] R. Palisetty, G. Eappen, J. L. G. Rios, J. C. M. Duncan, S. Domouchtsidis, S. Chatzinotas, B. Ottersten, B. Cortazar, S. D'Addio, and P. Angeletti, "Area-power analysis of FFT based digital beamforming for GEO, MEO, and LEO scenarios," in *Proc. IEEE 95th Veh. Technol. Conf. (VTC-Spring)*, Jun. 2022, pp. 1–5.

[37] A. Madanayake, R. J. Cintra, N. Akram, V. Ariyarathna, S. Mandal, V. A. Coutinho, F. M. Bayer, D. Coelho, and T. S. Rappaport, "Fast radix-32 approximate DFTs for 1024-beam digital RF beamforming," *IEEE Access*, vol. 8, pp. 96613–96627, 2020.

[38] W. Li, T. Wang, and X. Lan, "Codebook based beamforming in MIMO broadcast channels with finite rate feedback," in *Proc. 1st Int. Conf. Inf. Sci. Eng.*, 2009, pp. 2582–2585.

[39] B. Strait, "Antenna arrays with partially tapered amplitudes," *IEEE Trans. Antennas Propag.*, vol. AP-15, no. 5, pp. 611–617, Sep. 1967.

JUAN ANDRÉS VÁSQUEZ-PERALVO (Member, IEEE) was born in Quito, Ecuador. He received the B.Eng. degree in electronics and telecommunications from Escuela Politécnica Nacional, Quito, the M.Sc. degree in wireless communication systems from The University of Sheffield, Sheffield, U.K., and the Ph.D. degree in communication systems from Universidad Politécnica de Madrid, Madrid, Spain. Currently, he is pursuing a post-doc in the SIGCOM research group of the Interdisciplinary Centre for Security, Reliability, and Trust (SnT) of the University of Luxembourg, Luxembourg. His research interests include phase array design for satellite communications, meta-surfaces, additive manufacturing, and lens antenna design.

JORGE QUEROL (Member, IEEE) was born in Forcall, Castelló, Spain, in 1987. He received the B.Sc. (+5) degree in telecommunication engineering, the M.Sc. degree in electronics engineering, the M.Sc. degree in photonics, and the Ph.D. degree (cum laude) in signal processing and communications from Universitat Politècnica de Catalunya-BarcelonaTech (UPC), Barcelona, Spain, in 2011, 2012, 2013, and 2018, respectively. His Ph.D. thesis was devoted to the development of novel anti-jamming and counter-interference systems for Global Navigation Satellite Systems (GNSS), GNSS-Reflectometry, and microwave radiometry. One of his outstanding achievements was the development of a real-time standalone pre-correlation mitigation system for GNSS, named FENIX, in a customized Software Defined Radio (SDR) platform. FENIX was patented, licensed and commercialized by MITIC Solutions, a UPC Spin-off Company. Since 2018, he has been with the SIGCOM Research Group, Interdisciplinary Centre for Security, Reliability, and Trust (SnT), University of Luxembourg, Luxembourg, and the Head of the Satellite Communications Laboratory. He is involved in several ESA and Luxembourgish national research projects dealing with signal processing and satellite communications. His research interests include SDR, real-time signal processing, satellite communications, 5G non-terrestrial networks, satellite navigation, and remote sensing. He received the Best Academic Record Award of the year in electronics engineering from UPC, in 2012, the First Prize of the European Satellite Navigation Competition (ESNC) Barcelona Challenge from the European GNSS Agency (GSA), in 2015, the Best Innovative Project of the Market Assessment Program (MAP) of EADA Business School, in 2016, the Award Isabel P. Trabal from Fundació Caixa d'Enginyers for its quality research during the Ph.D., in 2017, and the Best Ph.D. Thesis Award in remote sensing from the IEEE Geoscience and Remote Sensing (GRSS) Spanish Chapter, Spain, in 2019.

JORGE LUIS GONZÁLEZ RIOS (Member, IEEE) received the B.S. (Hons.), M.S., and Ph.D. degrees in telecommunications and electronics from the Technological University of Havana (CUJAE), Cuba, in 2006, 2009, and 2018, respectively. From September 2006 to July 2019, he was a Lecturer and a Researcher with the Research Center on Microelectronics (CIME), CUJAE. He visited the Seville Institute of Microelectronics (IMSE-CNM), Spain, in 2010, 2011, and 2012, and the Group of Microelectronics, Federal University of Itajubá (UNIFEI), Brazil, in 2013. He is currently with the Interdisciplinary Centre for Security, Reliability and Trust (SnT), University of Luxembourg. His research interests include RF/analog circuits, embedded systems, and wireless and satellite communications.

EVA LAGUNAS (Senior Member, IEEE) received the M.Sc. and Ph.D. degrees in telecommunications engineering from the Polytechnic University of Catalonia (UPC), Barcelona, Spain, in 2010 and 2014, respectively. She was a Research Assistant with the Department of Signal Theory and Communications, UPC, from 2009 to 2013. In 2009, she was a Guest Research Assistant with the Department of Information Engineering, University of Pisa, Italy. From November 2011 to May 2012, she held a Visiting Research appointment with the Center for Advanced Communications (CAC), Villanova University, Villanova, PA, USA. In 2014, she joined the Interdisciplinary Centre for Security, Reliability and Trust (SnT), University of Luxembourg, where she currently holds a Research Scientist position. Her research interests include radio resource management and general wireless networks optimization.

FLOR ORTÍZ (Member, IEEE) received the B.S. degree in telecommunications engineering and the M.S. degree in electrical engineering-telecommunications from Universidad Nacional Autónoma de México (UNAM), Mexico City, Mexico, in 2015 and 2016, respectively, and the Ph.D. degree in telecommunications engineering from Universidad Politécnica de Madrid (UPM), Madrid, Spain, in 2021. Her Ph.D. thesis focused on optimizing the design of very high throughput satellite systems, especially optimizing the cost per Gbps in orbit and managing radio resources for flexible payloads using different machine learning techniques, especially those based on reinforcement learning and supervised learning. In 2019, during the Ph.D. she performed a research period with the University of Bologna, Italy. She joined as a Research Associate with the Interdisciplinary Center for Security, Reliability and Trust (SnT), University of Luxembourg. Her research interests include implementing innovative machine learning techniques for operations in satellite communication systems.

VICTOR MONZON BAEZA (Member, IEEE) received the B.Sc., M.Sc., and Ph.D. degrees (Hons.) in electrical engineering from the University Carlos III of Madrid, Spain, in 2013, 2015, and 2019, respectively. He was a Visiting Student with the Communications Research Group, University of Southampton, in 2015. He was a Software Developer and a Project Manager of Industry for Defense and Space sectors with Indra and GMV. In 2022, he joined the Interdisciplinary Centre for Security, Reliability and Trust (SnT), University of Luxembourg, where he currently holds a Research Associate position. He has been a Collaborator with Universitat Oberta de Catalunya (UOC), since 2019. His research interests include wireless communications and signal processing, focusing on massive MIMO techniques, 5G, satellite communications, and ground segment dimensioning. He received the Best Master Thesis Awards and the Best Ph.D. Award, in 2014 and 2019, respectively.

GIANLUCA FONTANESI (Member, IEEE) received the B.Sc. and M.Sc. degrees in telecommunication engineering from Politecnico of Milan, Italy, in 2009 and 2012, respectively, and the Ph.D. degree from University College Dublin, in 2022. In 2022, he joined the Interdisciplinary Centre for Security, Reliability and Trust (SnT), University of Luxembourg. He has several years of industrial experience, focused on the development and testing of wireless systems, and air-to-ground communication. During the Ph.D., he was a member of the EIRSAT-1 Project, Ireland's first satellite. His research interests include future wireless networks, NTN, and potential applications of machine learning techniques. He is a member of COST INTERACT. He is a reviewer for several journals of the IEEE, including IEEE TRANSACTIONS ON VEHICULAR TECHNOLOGY, IEEE COMMUNICATION LETTERS, and IEEE ACCESS.

LUIS MANUEL GARCÉS-SOCORRÁS (Member, IEEE) received the B.S. degree in automation control engineering, the M.S. degree in digital systems, and the Ph.D. degree in electronics from the Technological University of Havana, Cuba, in 2006, 2011, and 2017, respectively. From September 2008 to March 2022, he was a Lecturer and a Researcher with the Automation and Computing Department, Technological University of Havana. He was a Visiting Researcher with the Seville Institute of Microelectronics (IMSE-CNM), Spain, in 2010, 2011, and 2013. From September 2014 to March 2015, he was a Visiting Researcher with the Group of Microelectronics, Federal University of Itajubá (INIFEI), Brazil, and from September to December 2017, as a Postdoctoral Researcher. Since April 2022, he has been a Research and Development Specialist with the Interdisciplinary Centre for Security, Reliability and Trust, University of Luxembourg. His research interests include digital signal processing, FPGAs, and embedded systems implementations of satellite communication applications.

JUAN CARLOS MERLANO DUNCAN (Senior Member, IEEE) received the Diploma degree in electrical engineering from Universidad del Norte, Barranquilla, Colombia, in 2004, and the M.Sc. and Ph.D. Diploma (cum laude) degrees from Universitat Politècnica de Catalunya (UPC), Barcelona, Spain, in 2009 and 2012, respectively. With UPC, he was responsible for the design and implementation of a radar system known as SABRINA, which was the first ground-based bistatic radar receiver using space-borne platforms, such as ERS-2, ENVISAT, and TerraSAR-X as opportunity transmitters (C and X bands). He was in charge of the implementation of a ground-based array of transmitters, which was able to monitor land subsidence with subwavelength precision. These two implementations involved FPGA design, embedded programming, and analog RF/Microwave design. In 2013, he joined Institute National de la Recherche Scientifique, Montreal, Canada, as a Research Assistant of design and implementation of cognitive radio networks employing software development and FPGA programming. He joined the SIGCOM research group of the Interdisciplinary Centre for Security, Reliability, and Trust (SnT) of the University of Luxembourg, Luxembourg since 2016, where he currently works as a Research Scientist leading the COMMLAB laboratory at the SIGCOM group working on SDR implementation of satellite and terrestrial communication systems. His research interests include wireless communications, remote sensing, distributed systems, frequency distribution and carrier synchronization systems, software-defined radios, and embedded systems.

SYMEON CHATZINOTAS (Fellow, IEEE) received the M.Eng. degree in telecommunications from the Aristotle University of Thessaloniki, Thessaloniki, Greece, in 2003, and the M.Sc. and Ph.D. degrees in electronic engineering from the University of Surrey, Guildford, U.K., in 2006 and 2009, respectively. He is currently a Full-Professor and the Deputy Head of the SIGCOM Research Group, Interdisciplinary Centre for Security, Reliability and Trust, University of Luxembourg, Esch-sur-Alzette, Luxembourg, and a Visiting Professor with the University of Parma, Parma, Italy. He has coauthored more than 400 technical papers in refereed international journals, conferences, and scientific books. He has been involved in numerous research and development projects with the Institute of Informatics Telecommunications, National Center for Scientific Research Demokritos, Institute of Telematics and Informatics, Center of Research and Technology Hellas, and the Mobile Communications Research Group, Center of Communication Systems Research, University of Surrey. His research interests include multiuser information theory, cooperative/cognitive communications, and wireless network optimization. He was a co-recipient of the 2014 IEEE Distinguished Contributions to Satellite Communications Award, the CROWNCOM 2015 Best Paper Award, and the 2018 EURASIP JWCN Best Paper Award. He is on the Editorial Board of the IEEE OPEN JOURNAL OF VEHICULAR TECHNOLOGY and the *International Journal of Satellite Communications and Networking*.

• • •